
FREDHOLM NEURAL NETWORKS FOR FORWARD AND INVERSE PROBLEMS IN ELLIPTIC PDES

Kyriakos Georgiou¹, Constantinos Siettos², and Athanasios N. Yannacopoulos^{3,*}

¹Department of Electrical Engineering and Information Technologies, *University of Naples “Federico II”*, Naples, Italy

²Department of Mathematics and Application “Renato Caccioppoli”, *University of Naples “Federico II”*, Naples, Italy

³Department of Statistics and Stochastic Modelling and Applications Laboratory, *Athens University of Economics and Business*, Athens, Greece

ABSTRACT

Building on our previous work introducing Fredholm Neural Networks (Fredholm NNs/ FNNs) for solving integral equations, we extend the framework to tackle forward and inverse problems for linear and semi-linear elliptic partial differential equations. The proposed scheme consists of a deep neural network (DNN) which is designed to represent the iterative process of fixed-point iterations for the solution of elliptic PDEs using the boundary integral method within the framework of potential theory. The number of layers, weights, biases and hyperparameters are computed in an explainable manner based on the iterative scheme, and we therefore refer to this as the Potential Fredholm Neural Network (PFNN). We show that this approach ensures both accuracy and explainability, achieving small errors in the interior of the domain, and near machine-precision on the boundary. We provide a constructive proof for the consistency of the scheme and provide explicit error bounds for both the interior and boundary of the domain, reflected in the layers of the PFNN. These error bounds depend on the approximation of the boundary function and the integral discretization scheme, both of which directly correspond to components of the Fredholm NN architecture. In this way, we provide an explainable scheme that explicitly respects the boundary conditions. We assess the performance of the proposed scheme for the solution of both the forward and inverse problem for linear and semi-linear elliptic PDEs in two dimensions.

Keywords: Explainable machine learning, Elliptic PDEs, Fredholm neural networks, Numerical analysis, Deep neural networks, Boundary conditions

1 Introduction

In recent years, both theoretical and technological advancements have laid the ground for major advancements in the field of scientific machine learning. Both forward and inverse problems in dynamical systems have been extensively studied, across multiple applications and domains. In particular, the introduction of PINNs [66] and neural operators such as DeepONet [57], as well as Fourier neural networks [52], graph-based neural operators [53, 46], random feature models [62], and RandONets [20] provide an arsenal of such scientific machine learning methods (for a review see, e.g., [41, 20]). Furthermore, other techniques that bridge methods from numerical analysis towards more explainable schemes have also been developed, such as Legendre neural networks ([59]), simulation-based techniques ([22]), Deep Ritz-Finite element methods ([29]) and recently Kolmogorov-Arnold neural networks [55]. These approaches have been applied to the solution of the forward problem for Ordinary/Algebraic differential equations (ODEs, DAEs) [58, 39, 43, 8, 19, 44], Partial Differential Equations (PDEs) [32, 66, 63, 50, 58, 7, 13, 4, 17, 13, 14, 23, 49, 51, 36],

*Corresponding author: ayannaco@aueb.gr

as well as to Partial Integro-differential Equations (PIDEs) [75, 74, 27, 18]. Similarly, seminal work has been done when considering Integral Equations (IEs) such as the Fredholm and Volterra IEs with applications in various domains (see e.g., [61]). Furthermore, IEs can be connected to ODEs and PDEs. In particular, the connection to PDEs is established via the Boundary Integral Equation (BIE) method (see e.g., [42, 35]). This connection has been considered in the context of neural networks in [54]. More recently, in [60] the Boundary Integral Type Deep Operator Network (BI-DeepONet) and Boundary Integral Trigonometric Deep Operator Neural Network (BI-TDONet) are developed, combining the DeepONet framework with the BIE framework to solve PDEs with an optimized training process. In [16, 30, 38, 65], the authors use loss functions based on the residual between the model prediction and integral approximations to estimate the solution to FIEs using the standard learning approach for DNNs. In [75] the authors introduce Neural Integral Equations, a machine learning framework for estimating integral operators. In [69], the authors presented Integral Neural Networks, which were applied to computer vision problems, and were based on the observation that a fully connected neural network layer essentially performs a numerical integration.

Despite the multitude of schemes and applications, the complexity of DNNs is known to give rise to the so called "black-box" effect training, meaning that the quantification of errors and the effect of the hyperparameters is a very difficult, or even an impossible task. In addition, the standard training approach via loss function optimization (which may even fail in some cases, as shown in [72]), leads to weights and biases that have practically no explainability. Therefore, very recently, researchers construct neural network architectures that learn by emulating iterative numerical analysis schemes. For example, based on the concept of Runge-Kutta NNs presented back in the 90s' [67], in [31, 1], the authors create deep neural networks, based on the Runge-Kutta family of integrators, to learn the solution of ODEs. In [12] the authors propose a recursively recurrent neural network (R2N2) superstructure that can learn numerical fixed point algorithms such as Krylov, Newton-Krylov and Runge-Kutta algorithms. On this line of research, in [45], the authors have introduced a hybrid scheme combining iterative numerical solvers in the Krylov-subspace with preconditioning with DeepONets for the solution of parametrized steady-state linear PDEs. Finally, in [76, 40], a hybrid approach called HINTS (Hybrid Iterative Numerical Transferable Solver) for the solution of PDEs has been proposed. This approach integrates relaxation methods such as Jacobi, Gauss-Seidel, and multigrid techniques, with DeepONets, to enhance the convergence behavior across eigenmodes. Of course, robust error analysis is of critical importance and an open challenging problem, in all aforementioned schemes. One of the most prevalent issues for the solution of PDEs, is the fact that machine learning methods, such as PINNs impose boundary conditions as constraints in the optimization problem. However, this can exhibit large errors near and on the boundaries (e.g., [27] studies such errors when considering Kolmogorov backward equations in credit risk). More generally, this issue exists in problems with more complex dynamics, as displayed in [47]. Recently, important work has been done regarding error analysis for PINNs (and related) models. For example, in [6] exact and approximate error bounds are given for PINNs solutions for non-linear first-order ODEs. In [33, 34] the authors provide upper bounds for the error incurred by PINNs that depend on the dynamics of the underlying PDE. Such analysis has been recently done for operator learning ([10]) and when combining with Runge-Kutta methods ([70]). Additional mathematically rigorous treatments of errors for some types of PINNs can be found e.g., in [9, 15]. We also note that recent work provides rigorous definitions and analysis of stability and convergence for PINNs ([24]) for PDEs. However, model architecture and hyperparameter tuning still relies mainly on ad hoc/heuristic approaches (see for example [73, 14, 23, 19, 2]).

Very recently in [26], we introduced Fredholm NNs, integrating DNNs with the theory of fixed point schemes in the Banach space, for the solution of IEs. Here, generalizing this explainable framework, we utilize the potential theory and the Boundary Integral Equation (BIE) method to construct explainable DNNs for the solution of forward and inverse problems for elliptic PDEs, which occur in a vast range of problems and applications, such as in fluid mechanics [28], optimal control [5], thermodynamics and quantum mechanics [64]. We refer to this construction as the Potential Fredholm Neural Network (PFNN). We provide a rigorous constructive convergence proof and error analysis of PFNNs for the interior of the PDE domain as well as for the boundary. This analysis relies on the approximation of the boundary function and the integral discretization scheme, which directly correspond to specific components of the PFNN architecture. In this way, we can analyze the contribution of each hyperparameter of the neural network to these errors. Finally, we extend this analysis to a family of important semi-linear elliptic PDEs, by constructing recurrent PFNNs, which reflect appropriate classical iterative schemes for the solution of such PDEs.

The structure of the paper is as follows: in section 2, we recall the main results pertaining to Potential Theory for PDEs and Fredholm NNs and develop the proposed Potential Fredholm Neural Network approach for linear elliptic PDEs. In section 3, we provide a proof for the error bounds associated with the proposed approach. In section 4, we extend the method to semi-linear elliptic PDEs, and in section 5 we outline the methodology which utilizes PFNNs to solve the inverse source problem. Finally, in section 6, we assess the performance of the scheme with examples for all the aforementioned methodologies.

2 Methodology

We present the methodology by detailing a rigorous construction of PFNNs for the Poisson and Helmholtz PDEs. For clarity, we also provide a brief reminder regarding Potential Theory and Fredholm Neural Networks, as introduced in [26]. We note that the approaches developed are applicable to any type of geometry for the domain and corresponding boundary. However, for the examples presented, we will be considering a 2D disc domain, with unit radius and the corresponding unit circle boundary. We defer the study of other geometries for future work, as the present work focuses on the introduction of the framework, showing its utility for accurate and explainable construction of DNNs for the solution of elliptic PDEs.

In what follows, we will be considering the Banach space $\mathcal{X} := \mathcal{C}(\Omega, \mathbb{R})$, endowed with the norm $\|f(x)\|_{\Omega} = \sup_{x \in \Omega} |f(x)|$, with $x \in \mathbb{R}^d$ and $\Omega \subset \mathbb{R}^d$ a compact domain, and the Hilbert space $\mathcal{H} := L^2(D; R)$ endowed with the inner product $\langle f, g \rangle = \int_{\Omega} f(x)g(x)dx$. We remark that the results are generalizable to other spaces, e.g., $\mathcal{C}(\Omega, \mathbb{R}^n)$ or Lebesgue spaces.

2.1 Potential Theory and Fredholm Neural Networks

We begin by recalling the following theorem:

Theorem 2.1 ([21]). *Consider the two-dimensional linear Poisson equation for $u(x)$:*

$$\begin{cases} \Delta u(x) = \psi(x), & \text{for } x \in \Omega \\ u(x) = f(x) & \text{for } x \in \partial\Omega. \end{cases} \quad (1)$$

Its solution can be written via the double layer boundary integral given by:

$$u(x) = \int_{\partial\Omega} \beta(y) \frac{\partial\Phi}{\partial n_y}(x, y) d\sigma_y + \int_{\Omega} \Phi(x, y) \psi(y) dy, \quad x \in \Omega, \quad (2)$$

where $\Phi(x, y)$ is the fundamental solution of the Laplace equation, n_y is the outward pointing normal vector to y , σ_y is the surface element at point $y \in \partial\Omega$, and $\frac{\partial\Phi}{\partial n_y} = n_y \cdot \nabla_y \Phi$. It can be shown that the following limit holds, as we approach the boundary:

$$\lim_{\substack{x \rightarrow x^* \\ x \in \Omega}} \int_{\partial\Omega} \beta(y) \frac{\partial\Phi}{\partial n_y}(x, y) d\sigma_y = u(x^*) - \frac{1}{2}\beta(x^*), \quad x^* \in \partial\Omega. \quad (3)$$

Hence, the function $\beta(x^*)$, defined on the boundary, must satisfy the Boundary Integral Equation (BIE):

$$\beta(x^*) = 2 \left(f(x^*) - \int_{\Omega} \Phi(x^*, y) \psi(y) dy \right) - 2 \int_{\partial\Omega} \beta(y) \frac{\partial\Phi}{\partial n_y}(x^*, y) d\sigma_y, \quad x^* \in \partial\Omega. \quad (4)$$

In [27], we used the above formulation to construct Fredholm NNs for the solution of the Fredholm Integral Equation which produces the boundary function $\beta(x)$, $x \in \partial\Omega$. For completeness, here we present the Fredholm Neural Network that is used for the solution of the forward problems for (4).

Definition 2.2 (Fredholm neural networks). Consider an operator $\mathcal{T} : \mathcal{X} \rightarrow \mathcal{X}$, acting on f as:

$$\mathcal{T}f(x) = g(x) + \int_{\mathcal{A}} K(x, z) f(z) dz, \quad (5)$$

which is non-expansive, i.e.,:

$$\|\mathcal{T}f_1 - \mathcal{T}f_2\|_{\mathcal{A}} \leq q \|f_1 - f_2\|_{\mathcal{A}}, \quad (6)$$

for some $q \leq 1$, and a grid $Z = \{z_1, \dots, z_N\}$. Consider also a sequence $\{\kappa_n\}$, $\kappa_n \in (0, 1)$, such that $\sum_n \kappa_n (1 - \kappa_n) = \infty$, and let $\kappa = \kappa_n$, for all n . Then, the M -layer Fredholm NN, replicating the Krasnoselskii-Mann iterations, is a Deep Neural Network with a one-dimensional input x , M hidden layers each with N nodes, a linear activation function and with the weights and biases given by:

$$W_1 = (\kappa g(z_1), \dots, \kappa g(z_N))^\top, \quad b_1 = (0, 0, \dots, 0)^\top \quad (7)$$

for the first hidden layer,

$$W_m = \begin{pmatrix} K_D(z_1) & K(z_1, z_2) \kappa \Delta z & \cdots & K(z_1, z_N) \kappa \Delta z \\ K(z_2, z_1) \kappa \Delta z & K_D(z_2) & \cdots & K(z_2, z_N) \kappa \Delta z \\ \vdots & \vdots & \ddots & \vdots \\ \vdots & \vdots & \vdots & \vdots \\ K(z_N, z_1) \kappa \Delta z & K(z_N, z_2) \kappa \Delta z & \cdots & K_D(z_N) \end{pmatrix}, \quad b_m = (\kappa g(z_1), \dots, \kappa g(z_N))^\top, \quad (8)$$

for the hidden layers $m = 2, \dots, M - 1$, where $K_D(z) := K(z, z) \kappa \Delta z + (1 - \kappa)$, and finally:

$$W_M = (K(z_1, x) \Delta z, \dots, K(z_{i-1}, x) \Delta z, K_D(x), K(z_{i+1}, x) \Delta z, \dots, K(z_N, x) \Delta z)^\top, \quad b_M = (\kappa g(x)) \quad (9)$$

for the final layer, assuming $z_i = x$. The output of the Fredholm NN approximates the solution to the Fredholm Integral Equation $f(x) = \mathcal{T}f(x)$.

2.2 The Potential Fredholm NN for the Poisson PDE

In the introduction of Fredholm NNs, we utilized this framework for the solution of the Laplace equation. This approach required writing the double layer potential integral using a novel representation that allows us to approach the boundary smoothly to handle the jump condition (3). Here, we begin by extending this to the linear Poisson PDE. Regarding this construction, recall that the Fredholm NN approximates the method of successive approximations for the solution of a Fredholm Integral Equation of the second kind. The BIE (4) is in this same form and therefore, a Fredholm NN is the first component of the proposed framework, followed by an additional layer that simulates the calculation performed by the new representation of the double layer potential. This is outlined in the following main result:

Proposition 2.3 (PFNN construction for the Poisson PDE). *The Poisson PDE (1) can be solved using a Fredholm NN, with $M + 1$ hidden layers, for which the final and output weights $W_{M+1} \in \mathbb{R}^{N \times N}$, $W_O \in \mathbb{R}^N$ are given by:*

$$W_{M+1} = I_{N \times N}, \quad W_O = (\mathcal{D}\Phi(x, y_1) \Delta \sigma_y, \mathcal{D}\Phi(x, y_2) \Delta \sigma_y, \dots, \mathcal{D}\Phi(x, y_N) \Delta \sigma_y)^\top, \quad (10)$$

where we define the simple operator $\mathcal{D}\Phi(x, y) := \left(\frac{\partial \Phi}{\partial n_y}(x, y) - \frac{\partial \Phi}{\partial n_y}(x^*, y) \right)$. The corresponding biases $b_{M+1} \in \mathbb{R}^N$ and $b_O \in \mathbb{R}$ are given by:

$$b_{M+1} = (-\beta(x^*), \dots, -\beta(x^*))^\top, \quad b_O = \frac{1}{2} \beta(x^*) + \int_{\partial \Omega} \beta(y) \frac{\partial \Phi(x^*, y)}{\partial n_y} d\sigma_y + \int_{\Omega} \Phi(x, y) \psi(y) dy, \quad (11)$$

where $x^* := (1, \phi) \in \partial \Omega$ is the unique point on the boundary corresponding to $x := (r, \phi) \in \Omega$.

Proof. In [26], we have demonstrated that a Fredholm NN with M hidden layers can be constructed to solve the integral equation (4), producing the estimate $\beta_M(x)$. We know that the fundamental solution of the Laplace equation satisfies $\Delta_y \Phi(x, y) = \delta(x - y)$ and is given by $\Phi(x, y) = \frac{1}{2\pi} \ln |x - y|$, for $n = 2$.

The double layer potential (see Theorem 2.1) is given by:

$$u(x) = \int_{\partial \Omega} \beta(y) \frac{\partial \Phi(x, y)}{\partial n_y} d\sigma_y + \int_{\Omega} \Phi(x, y) \psi(y) dy, \quad (12)$$

where β is a density defined on the boundary $\partial \Omega$, such that:

$$f(x) = \int_{\partial \Omega} \beta(y) \frac{\partial \Phi(x, y)}{\partial n_y} d\sigma_y + \int_{\Omega} \Phi(x, y) \psi(y) dy + \frac{1}{2} \beta(x), \quad \text{for } x \in \partial \Omega, \quad (13)$$

which can be written as a Fredholm Integral Equation as:

$$\beta(x) = 2 \left(f(x) - \int_{\Omega} \Phi(x, y) \psi(y) dy \right) - 2 \int_{\partial \Omega} \beta(y(s)) \frac{\partial \Phi(x, y)}{\partial n_y} d\sigma_y. \quad (14)$$

It can easily be shown that the kernel is non-expansive (see detailed calculations in section 6), as required under the Fredholm NN framework. Solving the BIE is the first step in the process.

Next, we proceed with the calculation of the double layer potential in order to retrieve the solution of the PDE. Our approach relies on the underlying mathematical computations employing the dynamics of the double layer potential as we approach the boundary. Consider $x = (r, \phi) \in \Omega$ and $x^* = (1, \phi) \in \partial \Omega$, such that $x \rightarrow x^*$, and we have:

$$u(x) = \int_{\partial \Omega} (\beta(y(s)) - \beta(x^*)) \frac{\partial \Phi(x, y(s))}{\partial n_y} ds + \beta(x^*) + \int_{\Omega} \Phi(x, y) \psi(y) dy, \quad (15)$$

where we have used:

$$\int_{\partial \Omega} \frac{\partial \Phi(x, y)}{\partial n_y} d\sigma_y = 1, \quad \text{for } x \in \Omega.$$

Similarly:

$$u(x^*) = \int_{\partial\Omega} (\beta(y) - \beta(x^*)) \frac{\partial\Phi(x^*, y)}{\partial n_y} d\sigma_y + \frac{1}{2}\beta(x^*) + \int_{\Omega} \Phi(x^*, y)\psi(y)dy, \quad (16)$$

where we have used that:

$$\int_{\partial\Omega} \frac{\partial\Phi(x^*, y)}{\partial n_y} d\sigma_y = \frac{1}{2}, \quad \text{for } x^* \in \partial\Omega.$$

Subtracting $u(x) - u(x^*)$ and simplifying, we obtain as we approach the boundary:

$$u(x) = \int_{\partial\Omega} (\beta(y(s)) - \beta(x^*)) \left(\frac{\partial\Phi(x, y)}{\partial n_y} - \frac{\partial\Phi(x^*, y)}{\partial n_y} \right) d\sigma_y + \frac{1}{2}\beta(x_0) + \int_{\partial\Omega} \beta(y) \frac{\partial\Phi(x^*, y)}{\partial n_y} d\sigma_y + \int_{\Omega} \Phi(x, y)\psi(y)dy. \quad (17)$$

The above can be simplified to:

$$u(x) = \int_{\partial\Omega} (\beta(y(s)) - \beta(x^*)) \left(\frac{\partial\Phi(x, y)}{\partial n_y} - \frac{1}{4\pi} \right) d\sigma_y + \frac{1}{2}\beta(x^*) + \int_{\partial\Omega} \frac{1}{4\pi}\beta(y)d\sigma_y + \int_{\Omega} \Phi(x, y)\psi(y)dy, \quad (18)$$

in the case of the Poisson PDE. The components of the expression can be used to construct the corresponding weights and biases of for the final hidden layer of the Potential Fredolm NN, as given in (10) and (11). \square

Remark 2.4. Throughout the remainder of this paper, we may refer to (18) as the Fredholm NN representation of the (double-layer) potential. From a mathematical standpoint, this representation allows us to approach the boundary without the abrupt effects of the explicit jump component that the double layer potential exhibits. Instead, we are able to use a consistent representation that holds both in the domain and that identically satisfies the boundary conditions, as required.

The result above is also illustrated in Fig. 1.

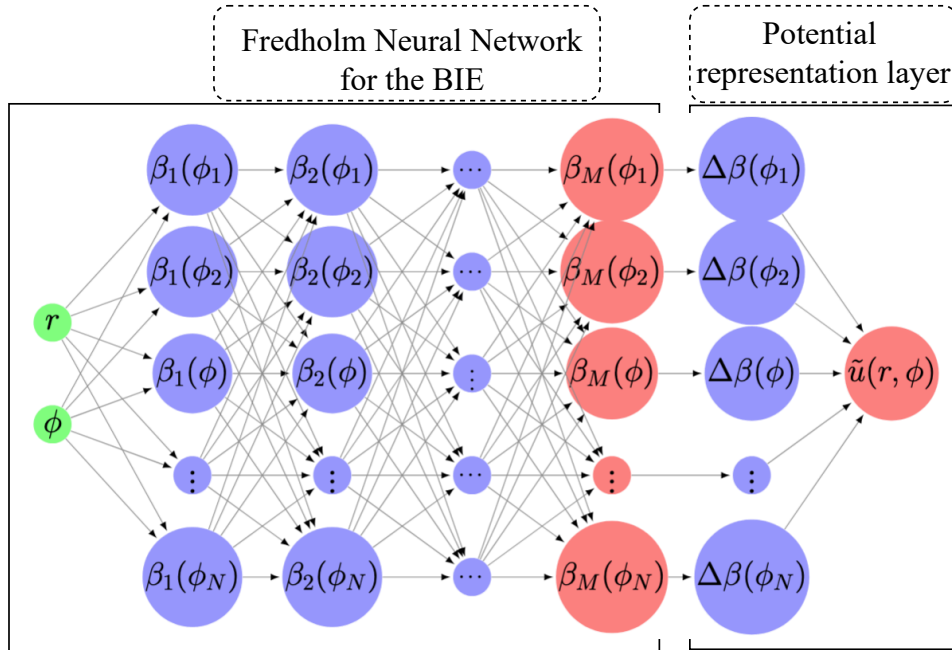


Figure 1: Schematic of the PFNN construction. The first component is a Fredholm Neural Network and the second encapsulates the representation of the double layer potential given in (18), decomposed into a the final hidden layer.

2.3 The Potential Fredholm NN for the Helmholtz PDE

We now consider the Helmholtz PDE, which is of the form:

$$\begin{cases} \Delta u(x) - \lambda u(x) = \psi(x), & x \in \Omega \\ u(x) = f(x), & x \in \partial\Omega. \end{cases} \quad (19)$$

Theorem 2.1 holds for the PDE (19), however the fundamental solution changes, and we have $\Phi(x, y) = -\frac{1}{2\pi} K_0(\lambda|x-y|)$, where K_0 is the modified Bessel function of the second kind (with index 0, in 2D space). Even though many of the calculations for the PFNN construction remain the same as in the linear Poisson PDE, we provide the detailed calculations below, as the change in the fundamental solution leads to different handling of the double layer potential formulation, and subsequent changes to the neural network construction. We now prove the following proposition.

Proposition 2.5. *The Helmholtz PDE (19) can be solved using a Fredholm NN with $M + 1$ hidden layers, where the first M layers solve the BIE (4) on a discretized grid of the boundary, y_1, \dots, y_N . The final hidden and output layers are constructed according to the Fredholm NN representation of the double layer potential for PDE (19), with weights $W_{M+1} \in \mathbb{R}^{N \times N}$, $W_O \in \mathbb{R}^N$ given by:*

$$W_{M+1} = I_{N \times N}, \quad W_O = (\mathcal{D}\Phi(x, y_1)\Delta\sigma_y, \mathcal{D}\Phi(x, y_2)\Delta\sigma_y, \dots, \mathcal{D}\Phi(x, y_N)\Delta\sigma_y)^\top, \quad (20)$$

where, $\mathcal{D}\Phi(x, y_i)$ as defined in Proposition 2.3. The corresponding biases $b_{M+1} \in \mathbb{R}^N$ and $b_O \in \mathbb{R}$ are given by:

$$b_{M+1} = (-\beta(x^*), \dots, -\beta(x^*))^\top, \quad (21)$$

$$b_O = \left(\frac{1}{2} + \int_{\Omega} \lambda \delta\Phi(x, y) dy \right) \beta(x^*) + \int_{\partial\Omega} \beta(y) \frac{\partial\Phi(x^*, y)}{\partial n_y} d\sigma_y + \int_{\mathcal{D}} \Phi(x, y) f(y) dy, \quad (22)$$

where we define $\delta\Phi(x, y) := \Phi(x, y) - \Phi(x^*, y)$.

Proof. It is known that the fundamental solution of the linear operator $\mathcal{L} := \Delta - \lambda$ satisfies:

$$\mathcal{L}\Phi(x, y) = \delta(x - y). \quad (23)$$

and is given by $\Phi(x, y) = -\frac{1}{2\pi} K_0(\sqrt{\lambda}|x-y|)$, where K_0 is the modified Bessel function of the second kind. The corresponding BIE is:

$$\beta(x) = 2 \left(f(x) - \int_{\Omega} \Phi(x, y) \psi(y) dy \right) - 2 \int_{\partial\Omega} \beta(y) \frac{\partial\Phi(x, y)}{\partial n_y} d\sigma_y. \quad (24)$$

It can be shown that the resulting kernel in the BIE (24) is indeed non-expansive. Furthermore, it is known from the properties of the Bessel function that the weak singularity can be treated numerically (more details are given in section 6). Now, the change in the differential operator creates a difference in the discontinuity dynamics. Hence, we will need to modify the calculations as we approach the boundary. To this end, we consider the following steps:

Step 1. Let $x \in \Omega$. Fix $\epsilon > 0$ and consider the ball centered at x with radiuses ϵ , such that $B(x, \epsilon) \subset \Omega$. In $\Omega - B(x, \epsilon)$, $\Phi(x, y)$ is smooth. We have:

$$0 = \int_{\partial\Omega} \mathcal{L}\Phi(x, y) d\sigma_y = \int_{\Omega - B(x, \epsilon)} \Delta_y \Phi(x, y) dy - \lambda \int_{\partial B(x, \epsilon)} \frac{\partial\Phi(x, y)}{\partial n_y} d\sigma_y. \quad (25)$$

By the Divergence Theorem, this becomes:

$$\begin{aligned} 0 &= \int_{\partial\Omega} \frac{\partial\Phi(x, y)}{\partial n_y} d\sigma_y - \lambda \int_{\partial B(x, \epsilon)} \frac{\partial\Phi(x, y)}{\partial n_y} d\sigma_y \\ &= \int_{\partial\Omega} \frac{\partial\Phi(x, y)}{\partial n_y} d\sigma_y + \int_{\partial B(x, \epsilon)} \frac{\partial\Phi(x, y)}{\partial n_y} d\sigma_y - \int_{\Omega - B(x, \epsilon)} \Phi(x, y) dy. \end{aligned} \quad (26)$$

Let us now consider the second term, where the outer unit normal to $\Omega - B(x, \epsilon)$ is $n_y = \frac{x-y}{|x-y|}$. Furthermore, note that $K_0(z) \sim -\ln(z)$ as $z \rightarrow 0$ (see e.g., [48]), and so we have:

$$\frac{\partial\Phi(x, y)}{\partial n_y} = \nabla_y \Phi(x, y) \cdot \frac{x-y}{|x-y|} \approx \frac{\sqrt{\lambda}}{2\pi} (\ln(\sqrt{\lambda}|x-y|))' ((y_1 - x_1)^2 + (y_2 - x_2)^2) = -\frac{1}{2\pi|x-y|}. \quad (27)$$

Thus, we obtain $\int_{\partial B(x,\epsilon)} \frac{\partial \Phi(x,y)}{\partial n_y} ds(y) \approx -1$, and therefore get:

$$\int_{\partial \Omega} \frac{\partial \Phi(x,y)}{\partial n_y} d\sigma_y = 1 + \int_{\Omega} \lambda \Phi(x,y) dy. \quad (28)$$

Step 2. Now, consider $x^* \in \partial \Omega$. We know that $\frac{\partial \Phi(x,y)}{\partial n_y}$ is not defined for $x^* = y$. Fix $x^* \in \partial \Omega$ and consider $B(x^*, \epsilon)$ and $\Omega_\epsilon \equiv \Omega - (\Omega \cap B(x, \epsilon))$. Furthermore, let $\Xi_\epsilon = \{y \in \partial B(x^*, \epsilon) : n_y \cdot (x^* - y) < 0\}$ and $\tilde{\Xi}_\epsilon = \partial \Omega_\epsilon \cap \Xi_\epsilon$. Then:

$$\begin{aligned} 0 &= \int_{\partial \Omega_\epsilon} \mathcal{L} \Phi(x^*, y) dy = \int_{\Omega_\epsilon} \Delta_y \Phi(x^*, y) dy - \int_{\partial \Omega_\epsilon} \frac{\partial \Phi(x^*, y)}{\partial n_y} d\sigma_y \\ &= \int_{\partial \Omega} \frac{\partial \Phi(x^*, y)}{\partial n_y} d\sigma_y + \int_{\tilde{\Xi}_\epsilon} \frac{\partial \Phi(x^*, y)}{\partial n_y} d\sigma_y - \int_{\Omega_\epsilon} \Phi(x^*, y) dy. \end{aligned} \quad (29)$$

In the above, n_y is the outer unit normal to Ω_ϵ . For $y \in \tilde{\Xi}_\epsilon$, $n_y = \frac{x^* - y}{|x^* - y|}$. Similar steps as before give:

$$\int_{\tilde{\Xi}_\epsilon} \frac{\partial \Phi(x^*, y)}{\partial n_y} d\sigma_y \approx \int_{\tilde{\Xi}_\epsilon} \frac{-1}{2\pi|x^* - y|} d\sigma_y \approx -\frac{1}{2\pi\epsilon} \left(\frac{1}{2} 2\pi\epsilon \right) = -\frac{1}{2}. \quad (30)$$

Therefore:

$$\int_{\partial \Omega} \frac{\partial \Phi(x^*, y)}{\partial n_y} d\sigma_y = -\frac{1}{2} + \int_{\Omega} \lambda \Phi(x^*, y) dy. \quad (31)$$

With the above results at hand, the double layer potential can be written as:

$$\begin{aligned} u(x) &= \int_{\partial \Omega} (\beta(y) - \beta(x^*)) \left(\frac{\partial \Phi(x,y)}{\partial n_y} - \frac{\partial \Phi(x^*,y)}{\partial n_y} \right) d\sigma_y \\ &\quad + \beta(x^*) \left(\frac{1}{2} + \int_{\Omega} \lambda \delta \Phi(x,y) dy \right) + \int_{\Omega} \Phi(x,y) \psi(y) dy + \int_{\partial \Omega} \beta(y) \frac{\partial \Phi(x^*, y(s))}{\partial n_y} d\sigma_y. \end{aligned} \quad (32)$$

□

As shown, in the case of the Helmholtz PDE, the difference in the fundamental solution creates an additional term in this new double layer potential representation. This, in turn, corresponds to a different bias term in the output of the constructed neural network. Indeed, as we will show in the next section, the properties of the fundamental solution, and by extension, its numerical integration, plays an important role in the approximation efficiency of the Fredholm NN.

3 Consistency and error analysis

In this section, we will provide bounds for the approximation errors associated with the given approach. Before proceeding with the rigorous treatment of the error bounds, we recall two important points: firstly, we note that the Fredholm NN replicates the process of successive approximations, which inherently introduces an approximation error $\|\beta_M - \beta\|$. Secondly, the solution constructed by the double layer potential satisfies identically the boundary condition when the BIE is satisfied. Therefore, based on these observations, it is expected that a stable scheme ensures that approximation errors at the boundary decrease progressively as the number of iterations increases.

Here, we provide bounds for these errors. Indeed, the Fredholm NN and subsequently the PFNN construction provide a framework where this is possible. This is an important step, since DNN-based models often lack consistent error estimates, and often exhibit relatively large errors on the boundaries.

For the completeness of the presentation, we recall the following proposition from [26].

Proposition 3.1. *Consider the integral equation $f(x) = (\mathcal{T}f)(x)$, where the integral operator:*

$$(\mathcal{T}f)(x) = g(x) + \int_{\mathcal{A}} K(x,z)f(z)dz, \quad (33)$$

is non-expansive and $\mathcal{A} := [a, b]$. Then, the error in the M -layer FNN approximation to the solution of the integral equation, f_M , satisfies the following bound:

$$\|f - f_M\|_{\mathcal{A}} \leq \frac{e^{1-q}}{1-q} \left(\|Tg - g\|_{\mathcal{A}} + \frac{D(b-a)^2}{2n} \right) e^{-(1-q)v_M}, \quad (34)$$

where $D = \max_{x \in \mathcal{A}} \frac{d}{dz} (K(x, z)g(z))$, $v_0 = 0$, $v_M = \sum_{\nu=0}^{M-1} \kappa$ (since in the Fredholm NN we consider constant values for the parameter in the Krasnoselskii-Mann iteration, $\kappa_{\nu} = \kappa$).

Given that the Fredholm NN replicates a discretization of the BIE, as well as the corresponding integrals in the proposed formula for the potential, it will be useful to use a notation for the discretization that encapsulates various schemes that may be considered. Throughout the proof, we will use the notation $\tilde{\int}_{\mathcal{A}}$ to represent the discretized version of $\int_{\mathcal{A}}$, for any arbitrary domain $\mathcal{A} \subseteq \mathbb{R}^n$ (in our case, $\mathcal{A} \subseteq \mathbb{R}$). We emphasize that this notation is useful so that the results that follow can be applied to any chosen discretization scheme.

We now demonstrate the main result pertaining to the errors bounds in the boundary conditions.

Theorem 3.2. Consider the PDE of the form (19), with a potential given in form (32) and corresponding BIE, (4), whose Fredholm NN approximation is given by $\beta_M(x) : \partial\Omega \rightarrow \mathbb{R}$. Furthermore, define the following terms, depending on the discretization scheme selected for the integrals in (32):

$$D_1(\mathcal{A}) := \left\| \int_{\Omega} \lambda \delta \Phi(x, y) dy - \tilde{\int}_{\Omega} \lambda \delta \Phi(x, y) dy \right\|_{\mathcal{A}}, \quad (35)$$

$$D_2(\mathcal{A}) := \left\| \int_{\Omega} \Phi(x, y) \psi(y) dy - \tilde{\int}_{\Omega} \Phi(x, y) \psi(y) dy \right\|_{\mathcal{A}}, \quad (36)$$

$$D_3(\mathcal{A}) := \left\| \int_{\partial\Omega} (\beta_M(y) - \beta_M(x^*)) \mathcal{D}\Phi(x, y) d\sigma_y - \tilde{\int}_{\partial\Omega} (\beta_M(y) - \beta_M(x^*)) \mathcal{D}\Phi(x, y) d\sigma_y \right\|_{\mathcal{A}}, \quad (37)$$

$$D_4(\mathcal{A}) := \left\| \int_{\partial\Omega} \beta_M(y) \frac{\partial \Phi(x, y)}{\partial n_y} d\sigma_y - \tilde{\int}_{\partial\Omega} \beta_M(y) \frac{\partial \Phi(x, y)}{\partial n_y} d\sigma_y \right\|_{\mathcal{A}}, \quad (38)$$

when $x \in \mathcal{A}$. Then, the PFNN construction providing \tilde{u} , as approximation of the solution of the PDE, satisfies the following error bound:

$$\|u - \tilde{u}\|_{\Omega} \leq \|\beta - \beta_M\|_{\partial\Omega} \left(\frac{1}{2} + 2 \left\| \int_{\partial\Omega} \mathcal{D}\Phi(x, y) d\sigma_y \right\|_{\Omega} + \left\| \int_{\Omega} \lambda \delta \Phi(x, y) dy \right\|_{\Omega} + \left\| \int_{\partial\Omega} \frac{\partial \Phi(x, y)}{\partial n_y} d\sigma_y \right\|_{\Omega} \right) + \|\beta_M\| D_1(\Omega) + D_2(\Omega) + D_3(\Omega) + D_4(\Omega). \quad (39)$$

Furthermore, the following inequality holds for errors on the boundary, $x \in \partial\Omega$:

$$\|f - \tilde{u}\|_{\partial\Omega} \leq \|\beta - \beta_M\|_{\partial\Omega} \left(\frac{1}{2} + \left\| \int_{\partial\Omega} \frac{\partial \Phi(x^*, y)}{\partial n_y} d\sigma_y \right\|_{\partial\Omega} \right) + D_2(\partial\Omega) + D_4(\partial\Omega), \quad (40)$$

where $\|\beta - \beta_M\|_{\partial\Omega}$ is the error in the FNN approximation of the boundary function β , as given in (34).

Proof. The proof entails decomposing the error into the components arising from the Fredholm NN estimator and the subsequent PFNN construction. Both of these are directly associated to well-known numerical methods with well-defined error bounds, which we can now take advantage of in the context of Fredholm NNs.

Considering the potential formulation (32) and keeping the notation $\mathcal{D}\Phi(x, y) := \frac{\partial\Phi}{\partial n_y}(x, y) - \frac{\partial\Phi}{\partial n_y}(x^*, y)$, we can write:

$$\begin{aligned}
\|u - \tilde{u}\|_{\Omega} &\leq \left\| \int_{\partial\Omega} (\beta(y) - \beta(x^*)) \mathcal{D}\Phi(x, y) d\sigma_y - \int_{\partial\Omega} (\beta_M(y) - \beta_M(x^*)) \mathcal{D}\Phi(x, y) d\sigma_y \right\|_{\Omega} \\
&+ \left\| \beta(x^*) \left(\frac{1}{2} + \int_{\Omega} \lambda \Delta\Phi(x, y) dy \right) - \beta_M(x^*) \left(\frac{1}{2} + \int_{\Omega} \tilde{\lambda} \Delta\Phi(x, y) dy \right) \right\|_{\Omega} \\
&+ \left\| \int_{\Omega} \Phi(x, y) \psi(y) dy - \int_{\Omega} \tilde{\Phi}(x, y) \psi(y) dy \right\|_{\Omega} \\
&+ \left\| \int_{\partial\Omega} \beta(y) \frac{\partial\Phi(x, y)}{\partial n_y} d\sigma_y - \int_{\partial\Omega} \beta_M(y) \frac{\partial\Phi(x, y)}{\partial n_y} d\sigma_y \right\|_{\Omega}. \tag{41}
\end{aligned}$$

We now consider each of the terms in the above expression separately. For clarity, in the steps below we gather the terms corresponding to the integral discretization errors and subsequently handle these using the well-known results for discretized integrals:

1st term:

$$\begin{aligned}
&\left\| \int_{\partial\Omega} (\beta(y) - \beta(x^*)) \mathcal{D}\Phi(x, y) d\sigma_y - \int_{\partial\Omega} (\beta_M(y) - \beta_M(x^*)) \mathcal{D}\Phi(x, y) d\sigma_y \right\|_{\Omega} \\
&\leq \left\| \int_{\partial\Omega} \left((\beta(y) - \beta_M(y)) + (\beta_M(x^*) - \beta(x^*)) \right) \mathcal{D}\Phi(x, y) d\sigma_y \right\|_{\Omega} \\
&+ \left\| \int_{\partial\Omega} (\beta_M(y) - \beta_M(x^*)) \mathcal{D}\Phi(x, y) d\sigma_y - \int_{\partial\Omega} (\beta_M(y) - \beta_M(x^*)) \mathcal{D}\Phi(x, y) d\sigma_y \right\|_{\Omega} \\
&\leq \int_{\partial\Omega} 2 \|\beta_M - \beta\|_{\partial\Omega} \mathcal{D}\Phi(x, y) d\sigma_y + D_3(\Omega) \leq 2 \|\beta_M - \beta\|_{\partial\Omega} \left\| \int_{\partial\Omega} \mathcal{D}\Phi(x, y) d\sigma_y \right\|_{\Omega} + D_3(\Omega), \tag{42}
\end{aligned}$$

where for the last steps we recall that the normal derivative of the fundamental solution is non-negative (see calculations for the potential above).

2nd term:

$$\begin{aligned}
&\left\| \beta(x^*) \left(\frac{1}{2} + \int_{\Omega} \lambda \delta\Phi(x, y) dy \right) - \beta_M(x^*) \left(\frac{1}{2} + \int_{\partial\Omega} \tilde{\lambda} \delta\Phi(x, y) dy \right) \right\|_{\Omega} \\
&\leq \frac{1}{2} \|\beta - \beta_M\|_{\partial\Omega} + \left\| \beta(x^*) \int_{\Omega} \lambda \delta\Phi(x, y) dy - \beta_M(x^*) \int_{\Omega} \lambda \delta\Phi(x, y) dy \right\|_{\Omega} \\
&+ \left\| \beta_M(x^*) \int_{\Omega} \lambda \delta\Phi(x, y) dy - \beta_M(x^*) \int_{\Omega} \tilde{\lambda} \delta\Phi(x, y) dy \right\|_{\Omega} \\
&\leq \|\beta - \beta_M\|_{\partial\Omega} \left(\frac{1}{2} + \left\| \int_{\Omega} \lambda \delta\Phi(x, y) dy \right\|_{\Omega} \right) + \|\beta_M\| D_1(\Omega). \tag{43}
\end{aligned}$$

3rd term:

$$\left\| \int_{\Omega} \Phi(x, y) \psi(y) dy - \int_{\Omega} \tilde{\Phi}(x, y) \psi(y) dy \right\|_{\Omega} =: D_2(\Omega). \tag{44}$$

4th term:

$$\begin{aligned}
& \left\| \int_{\partial\Omega} \beta(y) \frac{\partial\Phi(x, y)}{\partial n_y} d\sigma_y - \int_{\partial\Omega} \tilde{\beta}_M(y) \frac{\partial\Phi(x, y)}{\partial n_y} d\sigma_y \right\|_{\Omega} \\
& \leq \left\| \int_{\partial\Omega} \beta(y) \frac{\partial\Phi(x, y)}{\partial n_y} d\sigma_y - \int_{\partial\Omega} \beta_M(y) \frac{\partial\Phi(x, y)}{\partial n_y} d\sigma_y \right\|_{\Omega} \\
& + \left\| \int_{\partial\Omega} \beta_M(y) \frac{\partial\Phi(x, y)}{\partial n_y} d\sigma_y - \int_{\partial\Omega} \tilde{\beta}_M(y) \frac{\partial\Phi(x, y)}{\partial n_y} d\sigma_y \right\|_{\Omega} \\
& \leq \int_{\partial\Omega} \|\beta - \beta_M\|_{\partial\Omega} \frac{\partial\Phi(x, y)}{\partial n_y} d\sigma_y + D_4(\Omega) \leq \|\beta - \beta_M\|_{\partial\Omega} \left\| \int_{\partial\Omega} \frac{\partial\Phi(x, y)}{\partial n_y} d\sigma_y \right\|_{\Omega} + D_4(\Omega). \quad (45)
\end{aligned}$$

Hence, we obtain:

$$\begin{aligned}
\|u - \tilde{u}\|_{\Omega} \leq \|\beta - \beta_M\| & \left(\frac{1}{2} + 2 \left\| \int_{\partial\Omega} \mathcal{D}\Phi(x, y) d\sigma_y \right\|_{\Omega} + \left\| \int_{\Omega} \lambda \Delta\Phi(x, y) dy \right\|_{\Omega} + \left\| \int_{\partial\Omega} \frac{\partial\Phi(x, y)}{\partial n_y} d\sigma_y \right\|_{\Omega} \right) \\
& + \|\beta_M\|_{\partial\Omega} D_1(\Omega) + D_2(\Omega) + D_3(\Omega) + D_4(\Omega). \quad (46)
\end{aligned}$$

The error bound for the boundary condition follows directly from the above, by noticing the vanishing terms as $x \rightarrow x^*$. \square

The above result in combination with (34) provide an explicit expression for the error bounds in the PFNN construction, which depend on the boundary conditions of the PDE (via the BIE), the fundamental solution of the differential operator and the discretization of the integrals in the FNN representation of the potential. Through this composition, we are able to define the approximation errors in detail and quantify how or when larger errors may arise.

Therefore, within the proposed framework, we see that the error in the model approximation can be attributed to: a) the number of hidden layers in the Fredholm NN, which is equivalent to the number of iterations required to converge to the fixed point within a certain accuracy, and b) the number of nodes used to construct the FNN on which we approximate the solution of the PDE, and which are then used for the numerical integration. However, we also see that the error bound also depends explicitly on the boundary function $\|\beta_M\|$. This occurs from two components of expression (39) due to the error in the integral approximation. In particular, this dependency occurs through the term $\|\beta_M\| D_1(\Omega)$, as well as $D_4(\mathcal{A})$, where $\mathcal{A} = \Omega$ or $\partial\Omega$, since:

$$D_4(\mathcal{A}) \leq C \max_{x \in \mathcal{A}} \frac{d}{dy} \left(\beta_M(y) \frac{\partial\Phi(x, y)}{\partial n_y} \right) = C_1 \|\beta_M\|_{\mathcal{A}} + C_2, \quad (47)$$

by a simple application of the product rule, where $C > 0$ is a constant depending on the size of the discretization grid and $C_1, C_2 > 0$ are constants depending on the derivatives of $\frac{\partial\Phi(x, y)}{\partial n_y}$ and β_M , respectively. This decomposition of the errors therefore provides insight into how the form of the PDE can actually affect the error of the numerical approximation.

Finally, we note that the error analysis can be useful when considering the computational requirements for the construction of DNNs under the proposed framework. In particular, for a given computational cost, there exists a trade-off between the number of layers in the Fredholm NN for the approximation of the boundary function β_M , and the discretization of the integral terms; increasing the number of hidden layers in the Fredholm NN will ensure a smaller error $\|\beta_M - \beta\|$, thus decreasing the first four components in (39), but selecting a more computationally demanding numerical integration will decrease the final four terms. The selection of these hyperparameters can be done in a robust way since we know the components and how the underlying form of the PDE can affect the errors.

4 Recurrent PFNN construction for semi-linear elliptic PDEs

We now turn to the case of non-linear (semi-linear) elliptic PDEs of the form:

$$\begin{cases} \Delta u(x) = F(x, u(x)), & x \in \Omega \\ u(x) = f(x), & x \in \partial\Omega. \end{cases} \quad (48)$$

For their solution, fixed point schemes are often employed, which linearize the PDE at each step of the iteration. In line with this approach, we consider the monotone iteration scheme (see e.g., [11]), as below:

1. Choose a $\lambda > 0$ "sufficiently large" (see below)
2. Take an initial guess $u_0(x)$
3. Solve, for $n = 0, 1, 2, \dots$ the PDE:

$$\begin{cases} \Delta u_{n+1}(x) - \lambda u_{n+1}(x) = -\lambda u_n(x) + F(x, u_n(x)), & x \in \Omega, \\ u_{n+1}(x) = f(x), & x \in \partial\Omega. \end{cases} \quad (49)$$

Regarding the appropriate choice for λ , the value must be large enough to ensure the mapping:

$$T(u) = (\Delta - \lambda)^{-1}(-\lambda u + F(x, u)), \quad (50)$$

is a contraction, with the resulting iteration given by $u_{n+1} = T(u_n)$. By Banach's fixed point theorem, this ensures that the scheme converges to the solution of the PDE (see [11, 68] for such conditions and further details, and [3] for other iterative schemes).

This iterative scheme allows us to apply the proposed framework at each step of the scheme, whereby the source term will change at each iteration, in accordance to (49). We therefore refer to this as a Recurrent Potential Fredholm NN (RPFNN) construction.

Given that the source terms will depend on the solution $u_n(x)$, the numerical approximation of the integrals $\int_{\Omega} \Phi(x, y)\psi(y)dy$ must be considered. Here, we select a straightforward quadrature rule, across the points at which $u_n(x)$ has been calculated in order to avoid any interpolation-like approximations. For clarity, a full description of the fixed point algorithm solved via the FNN is given in Algorithm 1 and a schematic representation is given in Fig. 2.

Algorithm 1 Recurrent PFNN construction

Set number of iterations N' .
Set polar grid points $\mathcal{R} = \{r_1, \dots, r_{M_r}\}$ and $\Theta = \{\theta_1, \dots, \theta_{M_\theta}\}$.
Select parameter λ and initialize $u_0(x)$ (e.g., $u_0(x) = g(x)$).

Ensure: The approximated fixed-point solution $u^*(x)$

while $n \leq N'$ **do**

Step 1. Construct the PDE (49) with source term $\psi_n(x) := -\lambda u_n(x) + F(x, u_n(x))$.

Step 2. Approximate the integral with respect to the Poisson source term by:

$$\int_{\Omega} \Phi(x, y)\psi_n(y)dy \approx \sum_{r \in \mathcal{R}} \sum_{\theta \in \Theta} \Phi(x, r, \theta)\psi_n(r, \theta)r\Delta r\Delta\theta. \quad (51)$$

Step 3. Solve the BIE (24) via the FNN.

Step 4. Solve the PDE using the PFNN to estimate $u_n(r_i, \theta_j)$ for $i \in \{1, \dots, M_r\}, j \in \{1, \dots, M_\theta\}$.

Step 5. Set $n \rightarrow n + 1$.

end while

return $u_{N'}(x) \approx u^*(x)$.

Lemma 4.1. Consider the non-linear PDE (48), where $F(x, u)$ is C^1 with respect to $(x, u) \in \Omega \times \mathbb{R}$, and $\lambda > 0$ such that the mapping $T(u)$, as given in (50), is a q -contraction, with $q < 1$. Furthermore, let the approximation $\tilde{u}_n(x)$ be given by the Recurrent PFNN construction, as described in Algorithm 1, and with known $u_0(x)$. Then, the following error bounds hold:

$$\begin{cases} \|\tilde{u}_n - u\|_{\Omega} \leq \epsilon_{\Omega}^{PFNN} + q^n \|u_0 - u\|_{\Omega}, \\ \|\tilde{u}_n - f\|_{\partial\Omega} \leq \epsilon_{\partial\Omega}^{PFNN} + q^n \|u_0 - u\|_{\partial\Omega}, \end{cases} \quad (52)$$

where $\epsilon_{\Omega}^{RPFNN}, \epsilon_{\partial\Omega}^{RPFNN}$ denote the errors associated with the PFNN construction in the domain and on the boundary, as given by (39) and (40) respectively.

Proof. Notice that we can decompose the error into a component arising from the fixed point iterations and another due to the neural network approximation by writing $\|\tilde{u}_n - u\|_{\Omega} \leq \|\tilde{u}_n - u_n\|_{\Omega} + \|u_n - u\|_{\Omega}$. Substituting the error bound (39) and using the known error bound for the fixed point iterations results in (52). The error on the boundary follows in exactly the same fashion. \square

5 The Potential Fredholm Neural Network for Inverse Problems

To showcase the applications of the proposed framework, we now turn to the inverse problem for the family of PDEs examined in this paper. Here, we demonstrate how the proposed approach can be used to solve the inverse source

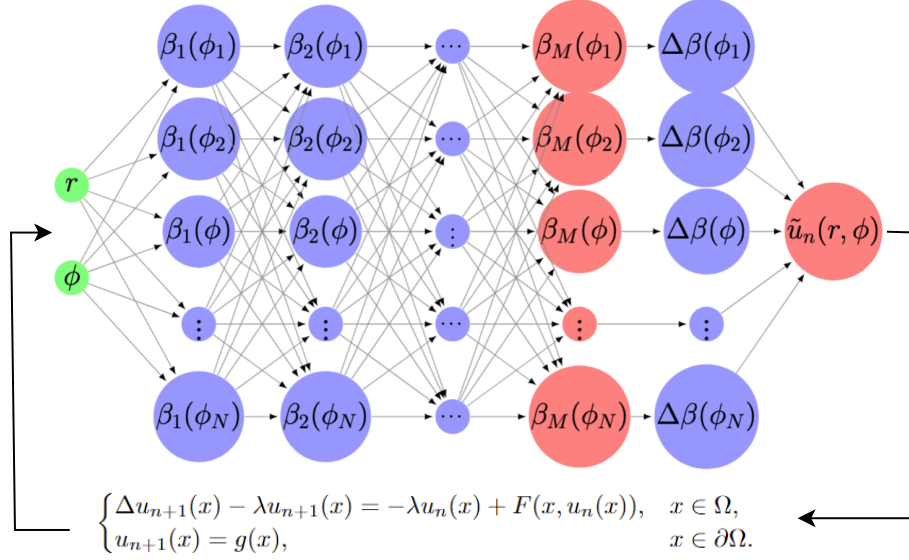


Figure 2: Schematic of the Recurrent Potential Fredholm NN to solve semi-linear elliptic PDEs.

problem for the Poisson PDE. Analogously, this framework can be applied to the other elliptic PDEs examined in this work; for brevity, we defer this for future examination.

We will be considering the inverse source problem for the PDE (1), consisting of a known boundary function $f : \partial\Omega \rightarrow \mathbb{R}$, as well as a coarse set of data points $\{u(x_i)\}_{i=1, \dots, n}$, $x_i \in \Omega$, and looking to approximate the unknown source function $\psi : \Omega \rightarrow \mathbb{R}$, using for a suitable model, represented by $\psi_\theta : \Omega \rightarrow \mathbb{R}$ with parameters θ (e.g., a shallow neural network), such that the data $\{\tilde{u}(x_i)\}$ and function $f(x)$ satisfy the Poisson PDE (1).

Note that the inverse source problem is well known to be an ill-posed problem, not admitting a unique solution. Indeed, there are infinitely many functions $\psi(x)$, $x \in \Omega$ that satisfy (1). Therefore, with this perspective, our goal is to learn the source term such that when used in the PDE, the resulting solution closely matches our data, rather than learning the exact source term function per se. This can now be studied within the framework of the PFNN; conceptually, the inverse problem consists of, given the data \tilde{u} , f , modelling the unknown source function, such that, when using the approximated source function in the forward PFNN, the resulting solution to the PDE, \hat{u} , is as close as possible to the given data \tilde{u} .

Our strategy takes advantage of the structure and convergence properties of the PFNN as follows: select a set of parameters θ such that when constructing the estimated kernel $\psi_\theta(\cdot, \cdot)$ and then feeding this into the PFNN with M hidden layers, denoted by $PFNN_M(\cdot; \psi_\theta)$, the output, $\hat{u}(x; \psi_\theta)$ (which will also be denoted $\hat{u}(x)$ for brevity), is as "close" as possible (in terms of an appropriately chosen loss function) to the given data \tilde{u} . The learning problem then reduces to the optimization problem of tuning the parameters θ appropriately until we reach the optimal set θ^* and the corresponding source model ψ_{θ^*} .

As mentioned, the described inverse problem is ill-posed. Hence, we require a regularization component. For our approach (and the example that is presented in section 6.2, where we use a shallow neural network model for the approximation ψ_θ), we apply a Tikhonov regularization, encapsulated by the term:

$$\mathcal{R}(\theta) = \|\psi_\theta\|_2^2, \quad (53)$$

where and the complete loss function is given by:

$$L(\theta) = \frac{1}{N} \sum_{i=1}^N \left(\tilde{u}(x_i) - \hat{u}(x_i; \psi_\theta) \right)^2 + \lambda_{reg} \mathcal{R}(\theta). \quad (54)$$

Training the model ψ_θ is done using a sparse grid of $u(x_i)$ values and we subsequently test the model on a larger grid over the domain Ω . Hence, in this way, we essentially learn the source term and simultaneously the full solution

Algorithm 2 PFNN for the inverse source problem

Ensure: Coarse grid $\{x_i\}_{i=1,\dots,N}$ and data $\tilde{u}(x_i)$, for $x_i \in \Omega$.

Create grid $\{x_i^b\}_{i=1,\dots,N'}$ and set the PFNN with nodes corresponding to $\{x_i^b\}$ and depth M .

Set number of training epochs N , initialize iterations, $n = 0$.

Approximate the unknown source $\psi(x)$ with model $\psi_{\theta^{(n)}}(x)$, where $\theta^{(n)}$ denotes the set of unknown parameters of the NN (weights and biases) at iteration n of training.

while $n \leq N$ **do**

Step 1. Construct a PFNN, $PFNN(x; \psi_{\theta^{(n)}})$.

Step 2. Use the PFNN output, $\hat{u}(x_i; \psi_{\theta^{(n)}})$ to calculate the model loss given by (54).

Step 3. Train model and set $n = n + 1$.

end while

return $\psi_{\theta^*}(x)$

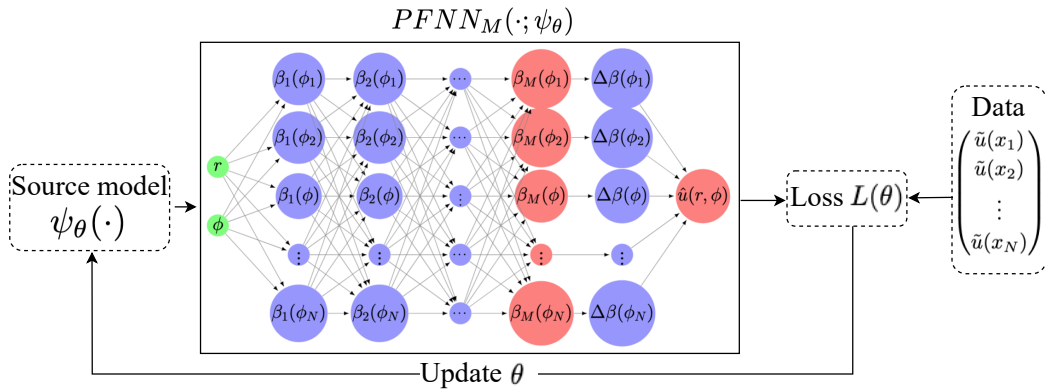


Figure 3: Schematic representation of Algorithm 2 to solve the inverse problem using the Potential FNN framework.

$u(x), x \in \Omega$, by passing through the Potential Fredholm NN. The approach is detailed in Algorithm 2 and shown schematically in Fig. 3.

We highlight that the structure of the PFNN itself ensures that we are simultaneously accounting for the data loss, as well as ensuring that the model adheres to the physics of the problem. This is an important novelty of the proposed method: rather than considering an arbitrary neural network structure and calculating the residuals of the PDE, a neural network with a pre-determined, numerical-analysis based architecture is used to ensure that the functions passed through it adhere to the given physics of the problem (in our case the PDE).

6 Numerical Implementation

In this section, we detail the numerical implementation of the neural network construction for the examples analyzed above. To this end, it is important to note that the fundamental solutions both for the Poisson as well as the Helmholtz operators exhibit weak singularities which, although integrable, can cause issues during the numerical estimation of the integrals which depend on them. We describe how these are handled to ensure high accuracy is maintained throughout the domain and boundary. With these examples we aim to show in detail how the theoretical framework presented above can be used to construct the PFNNs and can create accurate and explainable neural network models, whose properties and performance can be understood through the lens of classical numerical analysis for the solution of both forward and inverse problems of elliptic PDEs.

The calculations in the examples that follow were done in *Matlab*.

6.1 Solution of the Forward Problem

6.1.1 The Poisson PDE

Recall the form of the BIE (4). To construct the integral equation, we have $\frac{\partial \Phi(x, y)}{\partial n_y} = n_y \cdot \nabla_y \Phi(x, y)$, with $n_y = \frac{y}{|y|}$. Therefore:

$$\nabla_y \Phi(x, y) = \left(\frac{y_1 - x_1}{2\pi|x - y|^2}, \frac{y_2 - x_2}{2\pi|x - y|^2} \right),$$

and writing in terms of the arc-length parameterization we get:

$$\frac{\partial \Phi(x, y(\theta_2))}{\partial n_y} = \frac{r_2^2 - r_1 r_2 \cos(\theta_1 - \theta_2)}{2\pi|x - y|^2|y|}. \quad (55)$$

For the BIE in particular we have $x, y \in \partial\Omega$, and the kernel in the integral operator will become:

$$\frac{\partial \Phi(x, y(s))}{\partial n_y} = \frac{1 - \cos(\theta_1 - \theta_2)}{2\pi(2 - 2\cos(\theta_1 - \theta_2))} = \frac{1}{4\pi},$$

and, finally, the integral term is given by:

$$\begin{aligned} \int_{\Omega} \Phi(x, y) \psi(y) dy &= \int_0^{2\pi} \int_0^1 \frac{1}{2\pi} \ln|x - y| \psi(y) dy = \\ &= \int_0^{2\pi} \int_0^1 \frac{1}{2\pi} \ln((r_1 \cos \theta_1 - r_2 \cos \theta_2)^2 + (r_1 \sin \theta_1 - r_2 \sin \theta_2)^2)^{\frac{1}{2}} \psi(r_2, \theta_2) r_2 dr_2 d\theta_2. \end{aligned} \quad (56)$$

Written out explicitly, the BIE becomes:

$$\begin{aligned} \beta(x) &= 2 \left(f(x) - \int_0^{2\pi} \int_0^1 \frac{1}{2\pi} \ln((\cos \theta_1 - r_2 \cos \theta_2)^2 + (\sin \theta_1 - r_2 \sin \theta_2)^2)^{\frac{1}{2}} \psi(r_2, \theta_2) r_2 dr_2 d\theta_2 \right) \\ &\quad - 2 \int_{\partial\Omega} \beta(\theta) \frac{1}{4\pi} d\theta, \end{aligned} \quad (57)$$

and the final layer of the PFNN is as described in Proposition 2.3. As we have noted, the double integral in (56) is weakly singular at points within the integration domain. Hence, using naive numerical integration schemes may cause large errors. To account for this, we use an adaptive quadrature approach explicitly specifying the points at which singularities arise, i.e., at $r_2 = r_1$ and $\theta_2 = \theta_1$ (this specification can easily be implemented both in *Matlab* as well as *Python*). In this way, we compute the integral term required both for the BIE and for the final layer of the neural network in accordance to (18). Finally, the term $\int_{\partial\Omega} \frac{1}{4\pi} \beta(y(s)) ds$ in (18) is approximated with a simple Riemann sum on the selected grid that we use to estimate the boundary function $\beta(x)$.

Here, for our illustrations, we consider the following Poisson PDE:

$$\Delta u(x) = 2x_1, \quad (58)$$

on the unit disc, $\Omega = \{x \in \mathbb{R}^2 : x_1^2 + x_2^2 \leq 1\}$ with boundary condition $f(x) = 0$, for $x \in \partial\Omega$, for which, an analytical solution exists, and it is given by:

$$u(x) = \frac{1}{4} x_1 (x_1^2 + x_2^2 - 1). \quad (59)$$

We consider a ϕ -grid for the BIE of size $N = 1000$ to ensure sufficiently accurate approximation of the boundary function $\beta(x_i)$, for $x_i = (1, \phi_i)$, and an r -grid of size 100. To show the effect of the number of hidden layers in the FNN on the overall error in the solution of the PDE, we use various layers selections M in the estimation of the boundary function $\beta(x)$. The solution and error metrics L_∞ and Mean Absolute Error (MAE) are given in Fig. 4.

6.1.2 The Helmholtz PDE

For the PDE (19), the fundamental solution is given by $\Phi(x, y) = -\frac{1}{2\pi} K_0(\sqrt{\lambda}|x - y|)$. Hence, for $x = (x_1, x_2)$, $y = (y_1, y_2)$, we have that:

$$\frac{\partial \Phi(x, y)}{\partial y_1} = -\frac{\sqrt{\lambda}(y_1 - x_1)}{2\pi|x - y|} K_0'(\sqrt{\lambda}|x - y|) \quad (60)$$

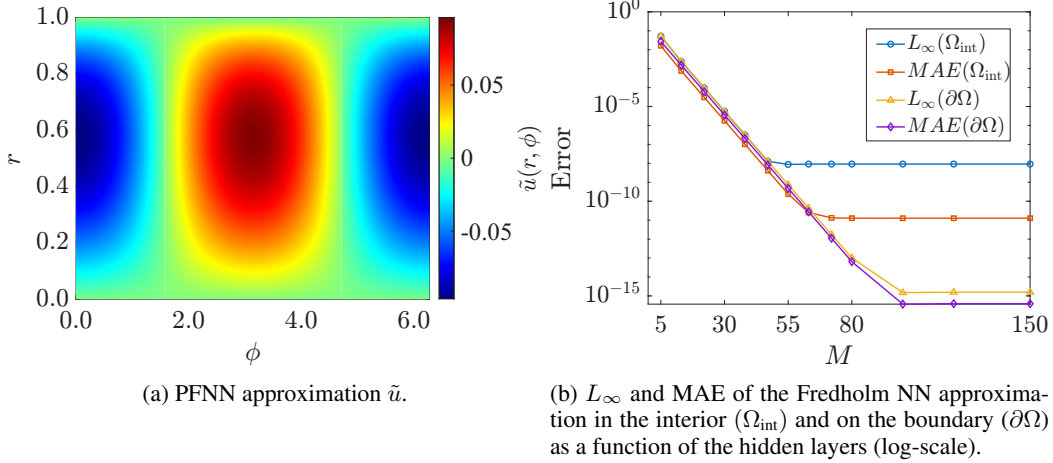


Figure 4: Results of the PFNN for the solution of the linear Poisson PDE (58).

and similarly for the derivative with respect to y_2 . Therefore, we obtain:

$$\frac{\partial \Phi(x, y)}{\partial n_y} = -\frac{\sqrt{\lambda} K'_0(\sqrt{\lambda}|x-y|)}{2\pi|x-y|} (y_1(y_1-x_1) + y_2(y_2-x_2)). \quad (61)$$

From the properties of the Bessel function, we know that $K'_0(x) = -K_1(x)$. Furthermore, we know that the Bessel function exhibits a singularity at $x = y$. We consider this separately. Firstly, for $x, y \in \partial\Omega, x \neq y$ we have:

$$\frac{\partial \Phi(x, y)}{\partial n_y} = \frac{\sqrt{\lambda} K_1(\sqrt{\lambda}|x-y|)}{2\pi|x-y|^2} (y_1(y_1-x_1) + y_2(y_2-x_2)) = \frac{\sqrt{\lambda} K_1(\sqrt{\lambda}|x-y|)}{4\pi|x-y|}. \quad (62)$$

In this case, as $x \rightarrow y$, for $x, y \in \partial\Omega$ the Bessel function exhibits a singularity and we therefore have a weakly singular kernel in the integral operator for the BIE (in contrast to the Poisson PDE, as seen above). As this affects the construction of the Fredholm NN, we examine the behavior of the kernel as $x \rightarrow y$. Specifically, we have that $K_0(z) \sim -\ln(z)$ (recall [48]). Then:

$$\Phi(x, y) \sim \frac{1}{2\pi} \ln(\sqrt{\lambda}|x-y|), \quad (63)$$

and so:

$$\frac{\partial \Phi(x, y)}{\partial n_y} = \frac{y_1(y_1-x_1) + y_2(y_2-x_2)}{2\pi|x-y|^2} = \frac{1}{4\pi}. \quad (64)$$

We therefore have a complete approach to numerically construct the kernel for the BIE, which takes into account the underlying mathematical theory of the fundamental solution. For our illustrations for this case, we consider the following linear PDE:

$$\Delta u(x) - \lambda u(x) = -x_1^3 + 2x_2^2 + 6x_1 - 4, \quad (65)$$

with $\lambda = 1$ on the unit disc, $\Omega = \{x_1, x_2 \in \mathbb{R} : x_1^2 + x_2^2 \leq 1\}$ with boundary condition $f(x) := x_1^3 + 2x_2^2 - 2$ for $(x_1, x_2) \in \partial\Omega$. For the above PDE, the analytical solution exists and reads:

$$u(x) = x_1^3 - 2x_2^2.$$

We consider a (r, ϕ) grid of size 100×1000 . For the numerical integration of $\int_{\Omega} \lambda \delta \Phi(x, y) dy$ as well as the additional term $\int_{\Omega} \Phi(x, y) \psi(y) dy$ the adaptive quadrature scheme as detailed above is used in order to handle the kernel singularities with high accuracy. The resulting solution and errors are shown in Fig. 5.

6.1.3 Semi-linear elliptic PDEs

We now turn to the recurrent structure to solve non-linear problems as described in section 4. For our illustrations, we consider the following 2D PDE:

$$\begin{cases} \Delta u(x) - e^u = -e^{1-x^2-y^2} - 4, & x \in \Omega \\ u(x) = 0, & x \in \partial\Omega, \end{cases} \quad (66)$$

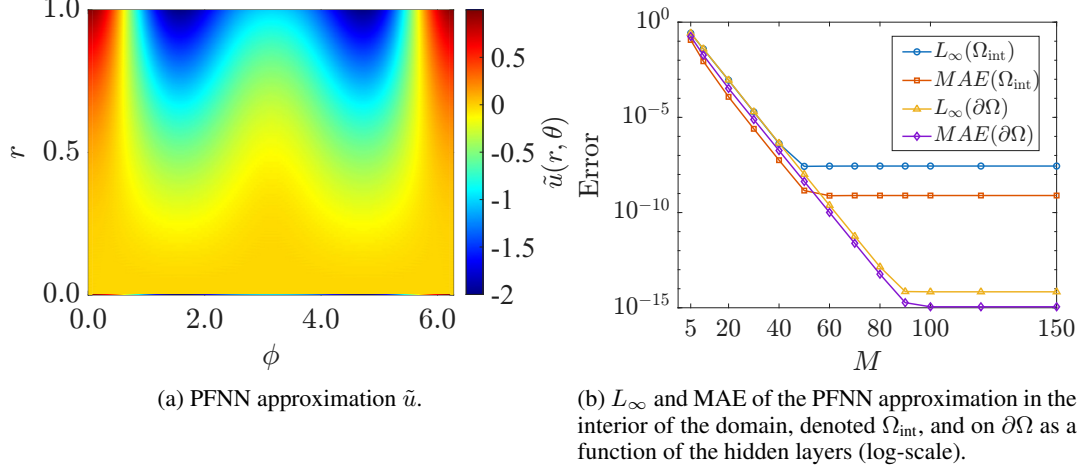


Figure 5: Results of the PFNN for the linear Helmholtz PDE (65).

which is in the form of the well-known and studied Liouville–Bratu–Gelfand equation (see e.g., ([25, 71, 37] for examples and further analysis). The above form is selected such that the analytical solution exists given by:

$$u(x_1, x_2) = 1 - (x_1^2 + x_2^2). \quad (67)$$

We construct the Recurrent PFNN, where in each iteration a PFNN with 100 hidden layers is used, and perform 12 iterations of Algorithm 1, with $\lambda = 1.0$. In Fig. 6 we display the results when using a (r, ϕ) grid of size 120×120 .

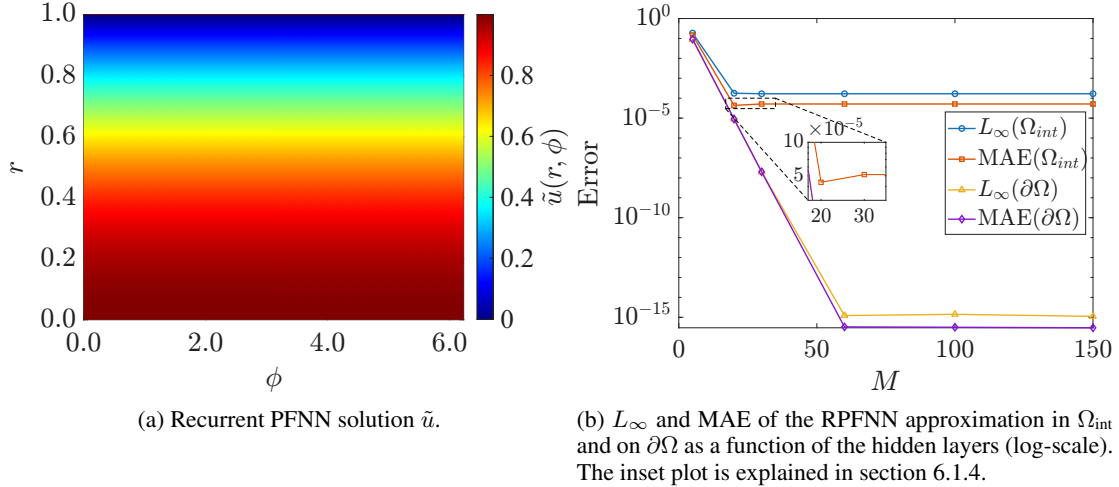


Figure 6: Results of the Recurrent Potential FNN construction for the PDE in (66).

The above examples show that the proposed framework is able to achieve highly accurate performance both in the interior and on the boundary of the domain. Of course, we note that alternative numerical integration schemes can also be considered and implemented within the PFNN construction.

6.1.4 Explainability

The benefits of the proposed approach lie primarily in its potential to better understand and, therefore, explain the source of errors as for example, those in Fig. 4b and 5b. In these two cases, we see that the errors decrease monotonically (though not necessarily strictly) with the number of hidden layers. This result is explainable given the results of Theorem 3.2, where we have shown that the error bound depends on the approximation $\|\beta - \beta_M\|$, as $M \rightarrow \infty$ (note that such a behaviour is not observed in PINNs in which case, the performance varies significantly when increasing the number of hidden layers).

However, it is also shown that the error bound (39) depends on $\|\beta_M\|$, i.e., the Fredholm NN approximation of the boundary function itself. Hence, since this value varies for different M , it is possible to observe larger errors as M increases, depending on the comparison between the terms depending on each of the two factors mentioned above.

Taking PDE (66) as an example, these error bounds allow us to interpret and explain the errors seen in Fig. 6b, where a very slight increase can be observed in the interior error metrics when considering the Recurrent PFNN approximations with $M = 20$ and $M = 30$. Specifically, let us consider the first iteration in the implementation described for (66). We have that $\|\beta_{M=20}\| = 1.0442995$, $\|\beta_{M=30}\| = 1.0443096$. This difference is translated into an increased error between the RPFNN approximation in each case, with $\|\tilde{u}_1 - u\| \approx 4.0794324\text{E}-01$ and $4.0794929\text{E}-01$ for $M = 20$ and $M = 30$, respectively. This difference in the error is then propagated throughout the remaining iterations of the RPFNN, as expected and in accordance with (52) (since the second term in the error bound is constant for both schemes). For larger M the error then remains constant, as the limit of both $\|\beta - \beta_M\|$ and $\|\beta_M\|$ has been reached.

These results indicate that, considering alternative mathematical formulations for the solution of PDEs that can be connected to a DNN model architecture, we can construct DNN models that adhere to explainable and interpretable behavior as hyperparameters, such as the number of hidden layers vary. We note that similar results hold for the number of nodes in the layers of the neural network (recall that in the RPFNN construction, the nodes correspond to the discretization of the integral in the BIE).

6.2 Solution of Inverse problems

For the illustration of the methodology outlined in section 5 we consider the Poisson PDE:

$$\Delta u(x) = \psi(x), \quad (68)$$

with boundary condition $f(x_1, x_2) = 2x_2, x \equiv (x_1, x_2) \in \partial\Omega$. Continuing to work in polar coordinates, we suppose we have data $\tilde{u}(r, \phi)$ over a (r, ϕ) -grid of size 20×20 and our goal is to estimate the unknown source term $\psi(x)$. For this illustrative example, we use training data $\tilde{u}(r, \phi)$ which is generated by the forward PFNN with $M = 100$ layers and 100 nodes per layer.

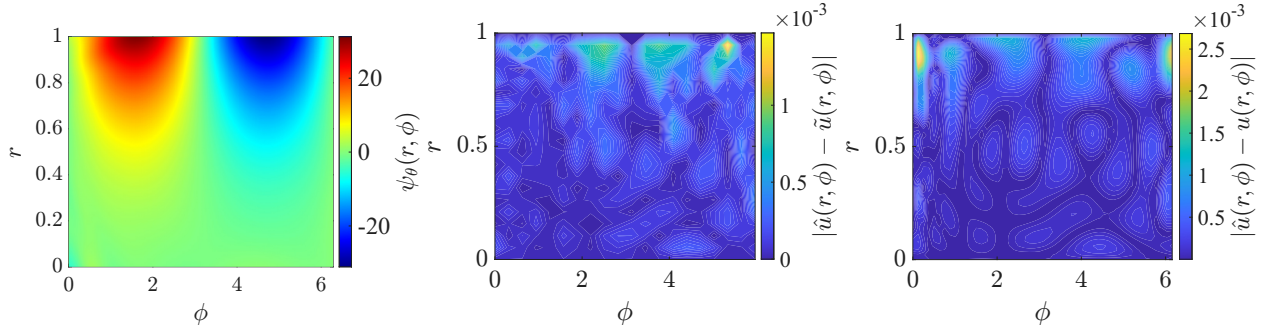
To solve the inverse problem, we consider a shallow neural network as the model for the unknown source term $\psi_\theta(x)$, with a single hidden layer, 20 nodes and a tanh activation function. Then, training is performed using Algorithm 2 where for the underlying PFNN we consider $M = 100$ layers to ensure convergence of the fixed-point scheme solving the BIE, with a ϕ -grid of size 100 corresponding to the interior nodes (we note that, of course, other hyperparameters of the Fredholm NN used for training can be chosen; we select these similar to our data generation for simplicity in this illustrative example). We perform 50 runs of this model training process using a Levenberg-Marquardt optimizer with 600 iterations, and a Tikhonov regularization constant $\lambda_{reg} = 1.0\text{E}-12$ (note that a small regularization is required here to ensure appropriate trade-off between the data loss and the regularizing term).

The average training MSE and L_∞ values are $8.45\text{E}-07$ and $3.39\text{E}-03$, respectively and the corresponding 10-90th percentile intervals are $[8.52\text{E}-08, 2.92\text{E}-06]$ and $[1.82\text{E}-03, 7.75\text{E}-03]$. Furthermore, we test the model on an unseen grid $\Omega_{test} := \{(r_i, \phi_j)\}_{i,j=1,\dots,50}$, over which the PDE is solved using the learned source function $\psi_\theta(x)$, producing $\hat{u}(\cdot; \hat{\theta})$ over the test grid. We compare the result to the true solution of the PDE, which is $u(x_1, x_2) = x_2(x_1^2 + x_2^2)(1 + x_1^2 + x_2^2)$. The average test MSE and L_∞ over all models are $1.72\text{E}-06$ and $7.73\text{E}-06$. Moreover, of particular importance are the errors on the boundary, where we know that $u(x_1, x_2) = f(x_1, x_2) = 2x_2$. As in the case of the forward problem, again we see that Fredholm NN applied to the inverse problem achieves extremely high accuracy on the boundary. We show a breakdown of the absolute error and L_∞ across the interior of the domain and the boundary in Table 1 (for brevity, these results are shown for the test grid; the results for the training grid are of the same order of magnitude).

Region	MAE = $\mathbf{mean} \hat{u} - u $		$L_\infty = \mathbf{max} \hat{u} - u $	
	Mean	[10th%, 90th%]	Mean	[10th%, 90th%]
Ω_{int}	7.03E-04	[3.36E-04, 1.49E-03]	7.73E-03	[3.70E-03, 1.47E-02]
$\partial\Omega$	1.95E-15	[1.41E-15, 2.50E-15]	5.26E-15	[3.89E-15, 7.55E-15]

Table 1: Error metrics across the 50 training runs in the interior and on the boundary of the test grid.

Finally, in Fig. 7 we display the contour of learned source term function corresponding to the model achieving the best training MSE ($6.70\text{E}-08$), along with the absolute error over the training and test grids. These results show not only a high accuracy in the resulting solution of the PDE, but also powerful generalization capability.



(a) The learned source term ψ_{θ^*} , where θ^* is the optimal set of model parameters. (b) Contour of the absolute error between the solution of the PDE using the learned source term and the training data, $|\hat{u} - \tilde{u}|$. (c) Contour of the absolute error between the solution of the PDE using the learned source term and the true solution on a test grid, $|\hat{u} - u|$.

Figure 7: Results of the inverse Poisson source problem (68).

7 Conclusions and Discussion

The concept of the representation of iterative numerical analysis algorithms with tailor-made deep neural network architectures dates back to 1990s’ as seen in [67], where a feedforward multilayer NN was used to implement the fourth-order Runge-Kutta method. This area of research remains active and is evolving towards numerical analysis-informed/ explainable deep learning models [31, 75, 56, 12]. The idea of the framework is to construct DNNs to directly model the iterative process, with its parameters reflecting the specific steps and coefficients of the numerical method. The weights and biases as well as other hyperparameters of the DNNs, are precomputed based on the iterative method, so no training on a loss function is necessary. This tailor-made *numerical analysis-informed* approach removes the curse of dimensionality arising in iterative optimization.

Within this line of research, we build upon the method that we introduced in [26] for solving integral equations and extend the framework by developing the Potential Fredholm Neural Network and the Recurrent Potential Fredholm NN for solving linear and semi-linear elliptic PDEs, both in the case of the forward and inverse problem. This method relies on the reformulation of classical numerical methods, such as fixed point iterations in the Banach space, and numerical integration schemes based on the boundary integral method (BIE), into the neural network framework. We show that the underlying mathematical theory can be used to construct a DNN for which we can also obtain a-priori, explainable error bounds that allow us to analyze the contributing factors that create these errors. In total, the proposed framework describes a method of constructing DNNs whose architecture is directly related to numerical methods and therefore significantly enhances model explainability, as well as accuracy. In our examples, we show that this approach achieves high accuracy throughout the domain and near-machine precision the boundary of the PDEs, thereby satisfying identically the boundary conditions, a strict requirement in the field of numerical methods for PDEs. By giving rigorous constructions and proofs of the convergence and error bounds, we showcase how custom neural network architectures can be used to solve issues such as the accuracy on the boundary without the need of hard-encoding the conditions, as well as interpretable (in the “classical” numerical methods sense) error analysis.

Concluding, we believe the proposed framework creates a path of interesting future research. Such directions include the high-dimensional PDEs, highly nonlinear systems and time-dependent PDEs, as well as applications in the field Scientific Machine Learning, such as Uncertainty Quantification (UQ).

Acknowledgements

K.G. acknowledges support from the PNRR MUR Italy, project PE0000013-Future Artificial Intelligence Research-FAIR. C.S. acknowledges partial support from the PNRR MUR Italy, projects PE0000013-Future Artificial Intelligence Research-FAIR & CN0000013 CN HPC - National Centre for HPC, Big Data and Quantum Computing, and from the GNCS group of INdAM. A.N.Y. acknowledges the use of resources from the Stochastic Modelling and Applications Laboratory, AUEB.

References

- [1] Georgios Akrivis, Charalambos G Makridakis, and Costas Smaragdakis. Runge-kutta physics informed neural networks: Formulation and analysis. *arXiv preprint arXiv:2412.20575*, 2024.
- [2] Erik L Bolager, Iryna Burak, Chinmay Datar, Qing Sun, and Felix Dietrich. Sampling weights of deep neural networks. *Advances in Neural Information Processing Systems*, 36, 2024.
- [3] Carlos Alberto Brebbia and Stephen Walker. *Boundary element techniques in engineering*. Elsevier, 2016.
- [4] Francesco Calabrò, Gianluca Fabiani, and Constantinos Siettos. Extreme learning machine collocation for the numerical solution of elliptic PDEs with sharp gradients. *Computer Methods in Applied Mechanics and Engineering*, 387:114188, 2021.
- [5] Eduardo Casas and Karl Kunisch. Optimal control of semilinear elliptic equations in measure spaces. *SIAM Journal on Control and Optimization*, 52(1):339–364, 2014.
- [6] Augusto T Chantada, Pavlos Protopapas, Luca Gomez Bachar, Susana J Landau, and Claudia G Scóccola. Exact and approximate error bounds for physics-informed neural networks. *arXiv preprint arXiv:2411.13848*, 2024.
- [7] Yifan Chen, Bamdad Hosseini, Houman Owhadi, and Andrew M Stuart. Solving and learning nonlinear pdes with gaussian processes. *Journal of Computational Physics*, 447:110668, 2021.
- [8] Mario De Florio, Enrico Schiassi, and Roberto Furfaro. Physics-informed neural networks and functional interpolation for stiff chemical kinetics. *Chaos: An Interdisciplinary Journal of Nonlinear Science*, 32(6), 2022.
- [9] Tim De Ryck and Siddhartha Mishra. Error analysis for physics-informed neural networks (pinns) approximating kolmogorov pdes. *Advances in Computational Mathematics*, 48(6):79, 2022.
- [10] Tim De Ryck and Siddhartha Mishra. Generic bounds on the approximation error for physics-informed (and) operator learning. *Advances in Neural Information Processing Systems*, 35:10945–10958, 2022.
- [11] Yuanhua Deng, Goong Chen, Wei-Ming Ni, and Jianxin Zhou. Boundary element monotone iteration scheme for semilinear elliptic partial differential equations. *Mathematics of computation*, 65(215):943–982, 1996.
- [12] Danimir T Doncevic, Alexander Mitsos, Yue Guo, Qianxiao Li, Felix Dietrich, Manuel Dahmen, and Ioannis G Kevrekidis. A recursively recurrent neural network (r2n2) architecture for learning iterative algorithms. *SIAM Journal on Scientific Computing*, 46(2):A719–A743, 2024.
- [13] Suchuan Dong and Zongwei Li. Local extreme learning machines and domain decomposition for solving linear and nonlinear partial differential equations. *Computer Methods in Applied Mechanics and Engineering*, 387:114129, 2021.
- [14] Suchuan Dong and Zongwei Li. A modified batch intrinsic plasticity method for pre-training the random coefficients of extreme learning machines. *Journal of Computational Physics*, 445:110585, 2021.
- [15] Nathan Doumèche, Gérard Biau, and Claire Boyer. Convergence and error analysis of pinns. *arXiv preprint arXiv:2305.01240*, 2023.
- [16] Sohrab Effati and Reza Buzhabadi. A neural network approach for solving fredholm integral equations of the second kind. *Neural Computing and Applications*, 21:843–852, 2012.
- [17] Gianluca Fabiani, Francesco Calabrò, Lucia Russo, and Constantinos Siettos. Numerical solution and bifurcation analysis of nonlinear partial differential equations with extreme learning machines. *Journal of Scientific Computing*, 89:44, 2021.
- [18] Gianluca Fabiani, Nikolaos Evangelou, Tianqi Cui, Juan M Bello-Rivas, Cristina P Martin-Linares, Constantinos Siettos, and Ioannis G Kevrekidis. Task-oriented machine learning surrogates for tipping points of agent-based models. *Nature communications*, 15(1):4117, 2024.
- [19] Gianluca Fabiani, Evangelos Galaris, Lucia Russo, and Constantinos Siettos. Parsimonious physics-informed random projection neural networks for initial value problems of odes and index-1 daes. *Chaos: An Interdisciplinary Journal of Nonlinear Science*, 33(4), 2023.
- [20] Gianluca Fabiani, Ioannis G Kevrekidis, Constantinos Siettos, and Athanasios N Yannacopoulos. Randonet: Shallow-networks with random projections for learning linear and nonlinear operators. *arXiv preprint arXiv:2406.05470*, 2024.
- [21] Gerald B Folland. *Introduction to partial differential equations*. Princeton university press, 2020.
- [22] Rüdiger Frey and Verena Köck. Deep neural network algorithms for parabolic pides and applications in insurance and finance. *Computation*, 10(11):201, 2022.

- [23] Evangelos Galaris, Gianluca Fabiani, Ioannis Gallos, Ioannis Kevrekidis, and Constantinos Siettos. Numerical bifurcation analysis of pdes from lattice boltzmann model simulations: a parsimonious machine learning approach. *Journal of Scientific Computing*, 92(2):1–30, 2022.
- [24] Dimitrios Gazoulis, Ioannis Gkanis, and Charalambos G Makridakis. On the stability and convergence of physics informed neural networks. *arXiv preprint arXiv:2308.05423*, 2023.
- [25] IM Gel et al. Some problems in the theory of quasilinear equations. *American Mathematical Society Translations: Series 2*, 29:295–381, 1963.
- [26] Kyriakos Georgiou, Constantinos Siettos, and Athanasios N Yannacopoulos. Fredholm neural networks. *SIAM Journal on Scientific Computing (to appear)*, 2025.
- [27] Kyriakos Georgiou and Athanasios N Yannacopoulos. Deep neural networks for probability of default modelling. *Journal of Industrial and Management Optimization*, pages 0–0, 2024.
- [28] David Gilbarg, Neil S Trudinger, David Gilbarg, and NS Trudinger. *Elliptic partial differential equations of second order*, volume 224. Springer, 1977.
- [29] Georgios Grekas and Charalambos G Makridakis. Deep ritz-finite element methods: Neural network methods trained with finite elements. *Computer Methods in Applied Mechanics and Engineering*, 437:117798, 2025.
- [30] Yu Guan, Tingting Fang, Diankun Zhang, and Congming Jin. Solving fredholm integral equations using deep learning. *International Journal of Applied and Computational Mathematics*, 8(2):87, 2022.
- [31] Yue Guo, Felix Dietrich, Tom Bertalan, Danimir T Doncevic, Manuel Dahmen, Ioannis G Kevrekidis, and Qianxiao Li. Personalized algorithm generation: A case study in learning ode integrators. *SIAM Journal on Scientific Computing*, 44(4):A1911–A1933, 2022.
- [32] Jiequn Han, Arnulf Jentzen, and E Weinan. Solving high-dimensional partial differential equations using deep learning. *Proceedings of the National Academy of Sciences*, 115(34):8505–8510, 2018.
- [33] Birgit Hillebrecht and Benjamin Unger. Certified machine learning: A posteriori error estimation for physics-informed neural networks. In *2022 International Joint Conference on Neural Networks (IJCNN)*, pages 1–8. IEEE, 2022.
- [34] Birgit Hillebrecht and Benjamin Unger. Rigorous a posteriori error bounds for pde-defined pinns. *IEEE Transactions on Neural Networks and Learning Systems*, 2023.
- [35] George C Hsiao and Wolfgang L Wendland. *Boundary integral equations*. Springer, 2008.
- [36] Bruno Jacob, Amanda A Howard, and Panos Stinis. Spikans: Separable physics-informed kolmogorov-arnold networks. *arXiv preprint arXiv:2411.06286*, 2024.
- [37] Jon Jacobsen and Klaus Schmitt. The liouville–bratu–gelfand problem for radial operators. *Journal of Differential Equations*, 184(1):283–298, 2002.
- [38] A Jafarian and S Measoomy Nia. Utilizing feed-back neural network approach for solving linear fredholm integral equations system. *Applied Mathematical Modelling*, 37(7):5027–5038, 2013.
- [39] Weiqi Ji, Weilun Qiu, Zhiyu Shi, Shaowu Pan, and Sili Deng. Stiff-pinn: Physics-informed neural network for stiff chemical kinetics. *The Journal of Physical Chemistry A*, 125(36):8098–8106, 2021.
- [40] Adar Kahana, Enrui Zhang, Somdatta Goswami, George Karniadakis, Rishikesh Ranade, and Jay Pathak. On the geometry transferability of the hybrid iterative numerical solver for differential equations. *Computational Mechanics*, 72(3):471–484, 2023.
- [41] George Em Karniadakis, Ioannis G Kevrekidis, Lu Lu, Paris Perdikaris, Sifan Wang, and Liu Yang. Physics-informed machine learning. *Nature Reviews Physics*, 3(6):422–440, 2021.
- [42] Oliver Dimon Kellogg. *Foundations of potential theory*, volume 31. Springer Science & Business Media, 2012.
- [43] Suyong Kim, Weiqi Ji, Sili Deng, Yingbo Ma, and Christopher Rackauckas. Stiff neural ordinary differential equations. *Chaos: An Interdisciplinary Journal of Nonlinear Science*, 31(9), 2021.
- [44] Benjamin C Koenig, Suyong Kim, and Sili Deng. Kan-odes: Kolmogorov–arnold network ordinary differential equations for learning dynamical systems and hidden physics. *Computer Methods in Applied Mechanics and Engineering*, 432:117397, 2024.
- [45] Alena Kopaničáková and George Em Karniadakis. Deepnet based preconditioning strategies for solving parametric linear systems of equations. *arXiv preprint arXiv:2401.02016*, 2024.
- [46] Nikola B Kovachki, Zongyi Li, Burigede Liu, Kamyar Azizzadenesheli, Kaushik Bhattacharya, Andrew M Stuart, and Anima Anandkumar. Neural operator: Learning maps between function spaces with applications to pdes. *J. Mach. Learn. Res.*, 24(89):1–97, 2023.

- [47] Aditi Krishnapriyan, Amir Gholami, Shandian Zhe, Robert Kirby, and Michael W Mahoney. Characterizing possible failure modes in physics-informed neural networks. *Advances in Neural Information Processing Systems*, 34:26548–26560, 2021.
- [48] Mary Catherine A Kropinski and Bryan D Quaife. Fast integral equation methods for the modified helmholtz equation. *Journal of Computational Physics*, 230(2):425–434, 2011.
- [49] Laura Laghi, Enrico Schiassi, Mario De Florio, Roberto Furfaro, and Domiziano Mostacci. Physics-informed neural networks for 1-d steady-state diffusion-advection-reaction equations. *Nuclear Science and Engineering*, 197(9):2373–2403, 2023.
- [50] Seungjoon Lee, Mahdi Kooshkbaghi, Konstantinos Spiliotis, Constantinos I Siettos, and Ioannis G. Kevrekidis. Coarse-scale pdes from fine-scale observations via machine learning. *Chaos: An Interdisciplinary Journal of Nonlinear Science*, 30(1):013141, 2020.
- [51] Seungjoon Lee, Yorgos M Psarellis, Constantinos I Siettos, and Ioannis G Kevrekidis. Learning black-and gray-box chemotactic pdes/closures from agent based monte carlo simulation data. *Journal of Mathematical Biology*, 87(1):15, 2023.
- [52] Zongyi Li, Nikola Kovachki, Kamyar Aizzadenesheli, Burigede Liu, Kaushik Bhattacharya, Andrew Stuart, and Anima Anandkumar. Fourier neural operator for parametric partial differential equations. *arXiv preprint arXiv:2010.08895*, 2020.
- [53] Zongyi Li, Nikola Kovachki, Kamyar Aizzadenesheli, Burigede Liu, Andrew Stuart, Kaushik Bhattacharya, and Anima Anandkumar. Multipole graph neural operator for parametric partial differential equations. *Advances in Neural Information Processing Systems*, 33:6755–6766, 2020.
- [54] Guochang Lin, Pipi Hu, Fukai Chen, Xiang Chen, Junqing Chen, Jun Wang, and Zuoqiang Shi. Binet: learning to solve partial differential equations with boundary integral networks. *arXiv preprint arXiv:2110.00352*, 2021.
- [55] Ziming Liu, Yixuan Wang, Sachin Vaidya, Fabian Ruehle, James Halverson, Marin Soljačić, Thomas Y Hou, and Max Tegmark. Kan: Kolmogorov-arnold networks. *arXiv preprint arXiv:2404.19756*, 2024.
- [56] Rainald Löhner and Harbir Antil. Neural network representation of time integrators. *International Journal for Numerical Methods in Engineering*, 124(18):4192–4198, 2023.
- [57] Lu Lu, Pengzhan Jin, Guofei Pang, Zhongqiang Zhang, and George Em Karniadakis. Learning nonlinear operators via deepnet based on the universal approximation theorem of operators. *Nature Machine Intelligence*, 3(3):218–229, 2021.
- [58] Lu Lu, Xuhui Meng, Zhiping Mao, and George Em Karniadakis. DeepXDE: a deep learning library for solving differential equations. *SIAM Review*, 63(1):208–228, 2021.
- [59] Susmita Mall and Snehashish Chakraverty. Application of legendre neural network for solving ordinary differential equations. *Applied Soft Computing*, 43:347–356, 2016.
- [60] Bin Meng, Yutong Lu, and Ying Jiang. Solving partial differential equations in different domains by operator learning method based on boundary integral equations. *arXiv preprint arXiv:2406.02298*, 2024.
- [61] Solomon Grigorevich Mikhlin. *Integral equations: and their applications to certain problems in mechanics, mathematical physics and technology*. Elsevier, 2014.
- [62] Nicholas H Nelsen and Andrew M Stuart. The random feature model for input-output maps between banach spaces. *SIAM Journal on Scientific Computing*, 43(5):A3212–A3243, 2021.
- [63] Guofei Pang, Liu Yang, and George Em Karniadakis. Neural-net-induced gaussian process regression for function approximation and pde solution. *Journal of Computational Physics*, 384:270–288, 2019.
- [64] Markus Poppenberg, Klaus Schmitt, and Zhi-Qiang Wang. On the existence of soliton solutions to quasilinear schrödinger equations. *Calculus of Variations and Partial Differential Equations*, 14(3):329–344, 2002.
- [65] Wenzhen Qu, Yan Gu, Shengdong Zhao, et al. Boundary integrated neural networks (binns) for acoustic radiation and scattering. *arXiv preprint arXiv:2307.10521*, 2023.
- [66] Maziar Raissi, Paris Perdikaris, and George E Karniadakis. Physics-informed neural networks: A deep learning framework for solving forward and inverse problems involving nonlinear partial differential equations. *Journal of Computational physics*, 378:686–707, 2019.
- [67] Ramiro Rico-Martinez, K Krischer, IG Kevrekidis, MC Kube, and JL Hudson. Discrete-vs. continuous-time nonlinear signal processing of cu electrodisolution data. *Chemical Engineering Communications*, 118(1):25–48, 1992.

- [68] J Sakakihara. An iterative boundary integral equation method for mildly nonlinear elliptic partial differential equations. *Brebbia, CA (Springer-Verlag, NY)*, pages 13–49, 1987.
- [69] Kirill Solodskikh, Azim Kurbanov, Ruslan Aydarkhanov, Irina Zhelavskaya, Yury Parfenov, Dehua Song, and Stamatios Lefkimmiatis. Integral neural networks. In *Proceedings of the IEEE/CVF Conference on Computer Vision and Pattern Recognition*, pages 16113–16122, 2023.
- [70] Jochen Stiasny and Spyros Chatzivasileiadis. Error estimation for physics-informed neural networks with implicit runge-kutta methods. *arXiv preprint arXiv:2401.05211*, 2024.
- [71] Yu-Qin Wan, Qian Guo, and Ning Pan. Thermo-electro-hydrodynamic model for electrospinning process. *International Journal of Nonlinear Sciences and Numerical Simulation*, 5(1):5–8, 2004.
- [72] Sifan Wang, Xinling Yu, and Paris Perdikaris. When and why pinns fail to train: A neural tangent kernel perspective. *Journal of Computational Physics*, 449:110768, 2022.
- [73] Tong Yu and Hong Zhu. Hyper-parameter optimization: A review of algorithms and applications. *arXiv preprint arXiv:2003.05689*, 2020.
- [74] Lei Yuan, Yi-Qing Ni, Xiang-Yun Deng, and Shuo Hao. A-pinn: Auxiliary physics informed neural networks for forward and inverse problems of nonlinear integro-differential equations. *Journal of Computational Physics*, 462:111260, 2022.
- [75] Emanuele Zappala, Antonio Henrique de Oliveira Fonseca, Josue Ortega Caro, Andrew Henry Moberly, Michael James Higley, Jessica Cardin, and David van Dijk. Neural integral equations. *arXiv preprint arXiv:2209.15190*, 2022.
- [76] Enrui Zhang, Adar Kahana, Alena Kopaničáková, Eli Turkel, Rishikesh Ranade, Jay Pathak, and George Em Karniadakis. Blending neural operators and relaxation methods in pde numerical solvers. *Nature Machine Intelligence*, pages 1–11, 2024.